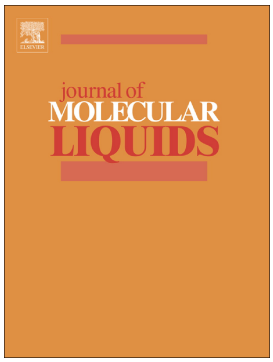

A wide potential window symmetric supercapacitor by TEMPO functionalized MWCNTs

Gomaa A.M. Ali, Elżbieta Megiel, Jan Romański, H. Algarni, Kwok Feng Chong

PII: S0167-7322(18)32556-X
DOI: doi:10.1016/j.molliq.2018.08.123
Reference: MOLLIQ 9568

To appear in: *Journal of Molecular Liquids*

Received date: 17 May 2018
Revised date: 20 August 2018
Accepted date: 22 August 2018

Please cite this article as: Gomaa A.M. Ali, Elżbieta Megiel, Jan Romański, H. Algarni, Kwok Feng Chong , A wide potential window symmetric supercapacitor by TEMPO functionalized MWCNTs. Molliq (2018), doi:10.1016/j.molliq.2018.08.123

A Wide Potential Window Symmetric Supercapacitor by TEMPO Functionalized MWCNTs

Gomaa A.M. Ali [a,b], Elżbieta Megiel [c,*], Jan Romański [c], H. Algarni [d,e], Kwok Feng Chong [a,*]

[a] Faculty of Industrial Sciences & Technology, Universiti Malaysia Pahang, Gambang, 26300 Kuantan, Malaysia

[b] Chemistry Department, Faculty of Science, Al–Azhar University, Assiut, 71524, Egypt

[c] University of Warsaw, Faculty of Chemistry, Pasteura 1, 02-093 Warsaw, Poland

[d] Research Centre for Advanced Materials Science (RCAMS), King Khalid University, Abha 61413, P. O. Box 9004, Saudi Arabia

[e] Department of Physics, Faculty of Sciences, King Khalid University, P. O. Box 9004, Abha, Saudi Arabia

* Corresponding author E-mail: ckfeng@ump.edu.my (K. F. Chong)

emegiel@chem.uw.edu.pl (E. Megiel)

Abstract

In this paper we report a simple and effective method to functionalize industrial-grade multi-walled carbon nanotubes (MWCNTs) with 2,2,6,6-tetramethylpiperidine-1-oxyl (TEMPO), *via* oxidation of $MWCNT_S$ and followed by carbodiimide coupling of amino-TEMPO. The effective coupling is confirmed and studied by EPR, HRTEM, BET, XPS, FTIR, TGA and XRD techniques. Electrochemical studies reveal the capacitive enhancement of MWCNTs-TEMPO, where MWCNTs-TEMPO shows capacitance value (66 F g^{-1} at 0.25 A g^{-1}) that is 5-times higher than that of industrial grade MWCNTs (13.5 F g^{-1} at 0.25 A g^{-1}). This can be due to the reversible redox reaction of nitroxide radicals on TEMPO that contributes to pseudocapacitance. A symmetrical supercapacitor is assembled with MWCNTs-TEMPO as electrode material and optimized with wide operating voltage (2 V) to produce high energy density of 26.6 Wh kg^{-1} with high stability (90% capacitance retention over 4000 cycles). The findings propose a facile approach to modify industrial grade MWCNTs as the electrode materials in supercapacitors.

Keywords: MWCNTs; Functionalization; Nitroxides; TEMPO; Supercapacitance.

1. Introduction

The structure of carbon nanotubes (CNTs) has been elucidated in 1991 [1], then to now, it has attracted considerable interdisciplinary research interests [2-4]. CNTs is a promising material as it has high length-to-diameter and surface area-to-volume aspect ratios [5]. Therefore it possesses superior mechanical, thermal, electrical, chemical and thermal properties as well as unique internal structures and low mass density [5, 6]. As a result of the interesting properties of CNTs, it is used for several applications such as catalysis [7], heavy ions and dye removal [3, 8], medical application [9], gas sensing [10], biosensors [11], supercapacitors [12, 13], solar cells [14] and construction materials additives [5]. CNTs can be prepared *via* different chemical methods such as; arc-discharge [1], laser vaporization [15], chemical vapor deposition [16], spray-pyrolysis [17] and flame pyrolysis [18]. Single-walled carbon nanotubes (SWCNTs) and multi-walled carbon nanotubes (MWCNTs) are the two main categories of CNTs [4, 19]. In addition, there are some other rare types such as double-walled carbon nanotubes (DWCNTs), fullerite, torus and nanoknot [20].

Many forms of carbon-based materials are widely used as supercapacitor electrode including graphene, carbon nanoparticles, carbon nanospheres, carbon nanofiber, C60, SWCNTs, DWCNTs and MWCNTs [13, 21-27]. Carbon materials possess electrical double layer capacitance (EDLC) which store charge on the electrode surface. CNTs is resplendent candidate for supercapacitor application as it has high surface area and good electrical conductivity. The electrochemical performance of CNTs can be enhanced by chemical activation or functionalization. Therefore, introducing new redox-active heteroatoms like oxygen, nitrogen and sulfur into carbon network can introduce pseudocapacitance in addition to the EDLC [28]. Composite materials from MWCNTs and polymers (polyaniline, polypyrrole and poly(3, 4-ethylenedioxythiophene) [29]) or metal oxides (MnO_2, NiO, Co_3O_4,) [30, 31] have also been studied as supercapacitor electrodes.

To fulfill global market demand, MWCNTs is often produced in bulk or in industrial grade. Such industrial-grade MWCNTs has serious agglomeration problem that leads to lower surface area. Therefore, industrial-grade MWCNTs is not favorable for electronic application, especially in the supercapacitor application as MWCNTs possesses low specific capacitance of 6 F g^{-1} [13]. In this context, surface functionalization of MWCNTs is necessary to improve its

electrochemical performance and charge storage capability. Functionalization of MWCNTs is found to be an efficient way of modification and it is divided into two categories: covalent and non-covalent functionalization. Covalent functionalization is a process of linking between functional entities and the carbon skeleton of nanotubes. Non-covalent functionalization is based on supramolecular complexation using different attractive forces, such as van der Waals, hydrogen bonds, electrostatic force and π-π stacking interactions [32, 33]. Functionalization of MWCNTs that integrates it into desired structures or attach to suitable nanostructures [11, 34], is essential to optimize its potential applications. Surface functional groups can modify MWCNTs surface charge, functionality and reactivity of the surface, and therefore increase its stability and dispensability in different phases [11, 35, 36]. Various studies have been conducted on functionalization of MWCNTs with different oxygen, nitrogen and sulfur containing groups such as carboxylic, amine, thiol, sulfonic, quinone, ether and hydroxyl [13, 36-38].

Nitroxides are paramagnetic and electrochemically active compounds with unpaired electron delocalized between nitrogen and oxygen atoms. The most prominent among the nitroxides compound is TEMPO stable nitroxide radical (2,2,6,6-tetramethylpiperidine-1-oxyl) [39]. This persistent radical has found many important applications primarily in organic synthesis, polymer chemistry, spectroscopy, biomedicine and material science [40, 41]. In recent years, much attention has been paid to the immobilization of TEMPO and its derivatives on various solid supports. Combination of properties derived from TEMPO and those originated from proper supports can lead to the interesting materials whose function can be turned into specific purposes. Within this, modification of MWCNTs seems to be especially promising because of its unique electronic, mechanical and chemical properties. Nevertheless, only a few examples of surface modification of MWCNTs with TEMPO derivatives were recently reported. Zhao et al. proposed [42] three-step protocol comprising oxidation of MWCNTs with HNO_3 and H_2SO_4 mixture, converting of carboxyl groups into corresponding chlorides using thionyl chloride and final formation of ester in reaction with TEMPO supported with –OH terminated spacer. Very recently, a four-step procedure for the synthesis of TEMPO functionalized MWCNTs was proposed [43]. The carbon nanotubes were oxidized with glutaryl peroxide followed by esterification of carboxyl groups with 3-bromopropanol and further substitution of halogen by azido groups. Finally, the azide/alkyne copper(I) catalyzed

"click" reaction with 4-propargyloxy-TEMPO was performed. All these reported processes are deemed unfavorable for industry due to their multiple steps and harsh conditions that could lead to low grafting density of TEMPO onto the surface.

In this study, we propose a facile two-step approach to functionalize industrial grade MWCNTs with TEMPO and its electrochemical performance as supercapacitor is evaluated.

2. Experimental techniques

2.1. Materials

Industrial-grade multi-wall carbon nanotubes (MWCNTs) were purchased from TCI. 4-Amino-2,2,6,6,-tetramethylpiperidinoxy free radical (98%) and N-(3-dimethylaminopropyl)-N′-ethylcarbodiimide (EDC) hydrochloride were purchased from Fluorochem, N-Hydroxysuccinimide (NHS) was purchased from Merck.

2.2. Samples preparation

2.2.1. Oxidation of MWCNTs

MWCNTs (4.4 g; earlier purified with 30% HCl for 40 min.) was added into the concentrated nitric acid (69%, 250 mL) solution and the suspension was sonicated for 5 min and purged with oxygen for 10 min. Then the mixture was refluxed for 12 h at 110 °C. After cooling to room temperature, the reaction mixture was diluted with 300 mL of deionized water and filtered under suction through a Schott funnel (G5 porosity). The functionalized MWCNTs was washed several times with water until the filtrate pH was close to neutral. The residue was dried in vacuum oven (25 mbar) at 65 ^{o}C for 16 h.

2.2.2. Synthesis of TEMPO functionalized MWCNTs

The suspension of oxidized MWCNTs (4 g) was sonicated for 5 min in DMF (300 mL), followed by activation in the excess of EDC (1.1 g) and NHS (0.7 g) and the suspension was then stirred for 2 h at room temperature. Subsequently, an excess of 4-amino-2,2,6,6,-tetramethylpiperidinoxy free radical (1.7 g) in DMF (100 mL) was added and the suspension was stirred at room temperature for 72 h. The product was isolated by filtration and washed

with DMF several times to remove unreacted substances. Finally, the TEMPO functionalized MWCNTs was washed with diethyl ether and dried to obtain 60% yield. The prepared material was denoted as MWCNTs-TEMPO. The functionalization process is depicted as Scheme 1.

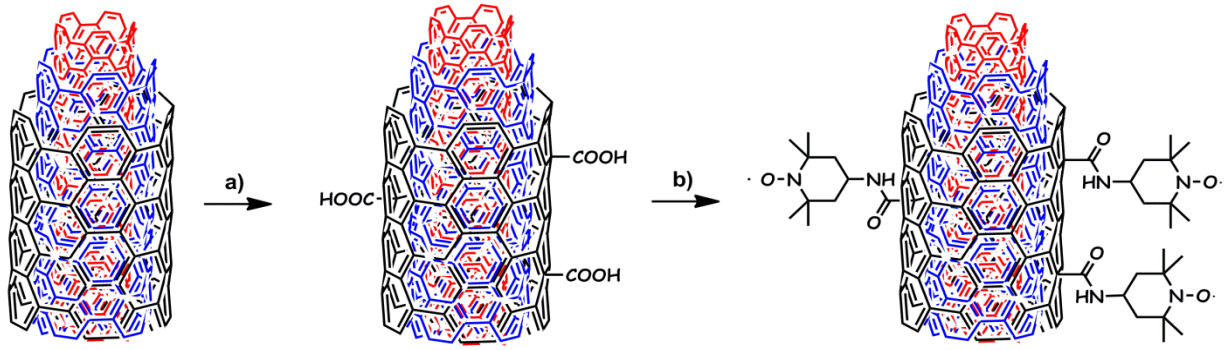

Scheme 1. The route to modification of MWCNTs with TEMPO; Reagents and conditions: a) HNO_3, 12 h, 110 °C, b) EDC hydrochloride, NHS, DMF, 2 h then 4–amino–2,2,6,6,–tetramethylpiperidinoxy, 72 h, room tempreature.

2.3. Samples characterization

Electron paramagnetic resonance (EPR) measurements were carried out at room temperature in solid state at X-band (9.3 GHz) using spectrometer Miniscope MS200 (Magnettech GmbH, Berlin, Germany). Modulation frequency was 100 kHz. X-ray photoelectron spectroscopy (XPS) measurements were done using a VG ESCALAB 210 electron spectrometer equipped with monochromatic Al-Kα source (1486.6 eV) of radiation. XPS data were calibrated using the binding energy of C 1s transition at 284.6 eV as the internal standard. Thermogravimetric analysis (TGA) measurements were performed under N_2 flow using DuPont 951 thermobalance (precision ±0.4%; minimal mass 0.02 mg) coupled with a DuPont 9900 thermal analyzer (heating rate 5 °C/min). Fourier transform infrared (FTIR) spectroscopy was performed on a Shimadzu FTIR model 8400S spectrophotometer. FTIR spectra were recorded with resolution 4 cm^{-1} from KBr pellets in a ratio of 1:1000 (w/w). High-resolution transmission electron microscopy (HRTEM) observations were carried out using FEI Talos F200X TEM with X-FEG cathode, an electron beam with a maximum energy of 200 keV, equipped with Bruker Super X EDX detector. The surface area of the materials was measured by NOVA 3200 surface area analyzer. The samples were obtained by casting the

aqueous suspension of sample (sonicated earlier for 10 minutes) onto a carbon coated nickel microgrid (200 mesh) and air-dried overnight. X-ray diffraction (XRD) patterns were collected on a Bruker D8 Discover diffractometer operating with Debye-Scherrer geometry. The measurements were performed using Cu-Kα radiation (λ = 1.540598 Å), at a scan rate of 1° min^{-1} in 0.012° steps, covering a range of 2θ from 10° to 90°.

2.4. Electrochemical measurements

For electrochemical characterization, the electrodes were prepared from the active material (MWCNTs-TEMPO), carbon black and polyvinylidene fluoride in the weight ratio of 90:5:5. The mixture was casted onto a nickel foam, dried and then uniaxially pressed at 5 tons. The electrochemical performance was investigated using three-electrode system which consists of active material as working electrode, Ag/AgCl (CH Instrument) as reference electrode and Pt wire (CH Instrument) as counter electrode.

A practical symmetrical supercapacitor was made by using two electrodes made of the active material that were electrically isolated from each other by a porous membrane pre-soaked with the electrolyte solution. It was then sandwiched and pressed into a coin cell design. The electrochemical data were collected using an AUTOLAB PGSTAT30 electrochemical workstation, equipped with frequency response analyzer. Cyclic voltammetry (CV) tests were performed in different potential ranges at different scan rates. Galvanostatic charge-discharge (CDC) tests were performed at different current densities. Electrochemical impedance spectroscopy (EIS) data were collected from 50 kHz to 0.01 Hz, at open circuit potential (OCP) with a.c. amplitude of 10 mV. To get equal ionic concentration, 2 M KOH and 1 M Na_2SO_4 were used as the electrolyte throughout electrochemical measurements.

3. Results and discussion

3.1. Structural and morphological analyses

The presence of nitroxides radicals attached to the MWCNTs-TEMPO was confirmed by EPR spectroscopy. As seen in Fig. S1, MWCNTs does not give any signal in the range in which TEMPO exhibits strong absorption. The EPR spectrum of MWCNTs-TEMPO was

recorded in the solid state. The high concentration of nitroxide attached to the nanotube surface can be confirmed by the broad singlet shape of the spectrum without visible superfine structure lines [44].

High-resolution TEM (HRTEM) image of MWCNTs-TEMPO (Fig. S2) shows the tubular morphology of MWCNTs. It is clearly to be seen that, the functionlization process causes no observable structural damage to MWCNTs. The diameter of the tubes is ranged from 20 nm to 80 nm and they are well separated from each other, probably due to the disruption of van der Waals forces resulting from TEMPO functionalization [19]. This can lead to higher ion diffusion within MWCNTs structure which directly contributes to higher specific capacitance. The TEMPO functionalization is random and evenly scattered onto MWCNTs surface, which can be seen from the EDX mapping in Fig. S2 inset.

Other indication of the non-damaged crystal structural of MWCNTs after TEMPO functionalization is seen in XRD analysis. XRD patterns of MWCNTs and MWCNTs-TEMPO are presented in Fig. S3. The pattern is typical for MWCNTs structure with the strongest peak at the angle of 26.2^{o} corresponding to (002) reflection of the hexagonal graphite structure (COD: 96-900-8570) [45]. There are also distinguishable other peaks of graphite at about 43.5^{o}, 44.5^{o}, 54.1^{o} and 77.8^{o} associated with (100), (101), (004), and (006) planes, respectively [20]. The sample after functionalization with TEMPO exhibits very similar XRD pattern, indicating that the TEMPO functionalization has not destroyed the crystal structure of MWCNTs. However, simple change in the peaks intensity due to the different absorption coefficients of the elements present in the functional groups [46].

N_2 adsorption-desorption isotherms of MWCNTs and MWCNTs-TEMPO are shown in Fig. S4 and the pore size distributions are shown as inset. Based on BET theory, MWCNTs and MWCNTs-TEMPO show high specific surface area (S_{BET}) values of 48.1 and 55.7 $m^2\ g^{-1}$, respectively, which is considered as a crucial parameter in the ion adsorption process in the electrochemical measurements. The higher S_{BET} for MWCNTs-TEMPO than that before functionalization, due to the fact that, the separation between tubes by the action of TEMPO groups. The total pore volume (V_p) of MWCNTs and MWCNTs-TEMPO are 0.18 and 0.21 $cm^3\ g^{-1}$, respectively. In addition, the average pore diameters (P_w) could be obtained as:

$P_w = 4V_p/S_{BET}$ [47, 48] and found to be 14.9 and 15.1 nm for MWCNTs and MWCNTs-TEMPO, respectively.

The presence of functional groups attached to the nanotube surface was confirmed by XPS (Fig. 1a-c). The wide survey XPS profile is shown in Fig. S5. The C 1s spectrum of the obtained MWCNTs-TEMPO is asymmetric with very long tail extended to higher energy. The fitted experimental data can be deconvoluted into several peaks. The main peak among them, is centered at 284.6 eV, which corresponds to the sp^2 hybridized carbons that are connected like in the graphite structure. The next Gaussian peaks can be assigned to the following bonds: C–C bonds and C–H bonds sp^3 carbons centered at 285.1 eV [49], C–N bonds at 289 eV [49] which confirms the functionalization of the surface with piperidine ring, C=O bond at 287.9 eV derived from the amide groups [50]. Notably, the peak centered at 285.1 eV can be partially attributed to the defects on nanotube structures [50]. According to the literature data, the peaks at 286.8 eV and 290.0 eV in C 1s spectrum, correspond to carbon atoms connected with hydroxyl and carboxyl groups, respectively [51]. Additionally, in the C 1s spectrum of the synthesized material, the π–π^* transition loss peak was observed at 290.8 eV and shake-up satellite at 291.6 eV.

The N 1s spectrum can be deconvoluted into two peaks centered at 400.0 eV and 401.9 eV, both with the same value of full-width at half-maximum (FWHM) 1.78 eV. The first peak could be attributed as common for N–O$^\bullet$ bonds and N–H bonds in the amide groups [41, 52, 53]. Considering atomic concentration of nitrogen atoms derived from quantitative analysis by using XPS (0.86%), the grafting density of TEMPO molecules on the nanotube surface is 0.58 mmol/g. The next peak in the N 1s spectrum (401.9 eV) can be assigned to a shake-up satellite involving N–O$^\bullet$ bonds in analogy to those observed for TEMPO immobilized on the other solid supports such nanoparticles and thin films [52, 54]. The O 1s spectrum can be deconvoluted into three peaks centered at 531.5 eV attributed to the oxygen atom in the carbonyl group [55], 533.6 eV corresponds very well to the oxygen atom in the nitroxide group [54] and 536.7 eV most likely resulted from the presence of water molecules adsorbed on the surface of carbon nanotubes.

Interestingly, the atomic concentration of oxygen atoms corresponding to the carbonyl groups (1.77%) is not equal to the atomic concentration of oxygen belonging to the nitroxide

groups (1.44%). This divergence indicates that other functional groups such as –OH or unreacted –COOH are attached to the MWCNTs surface.

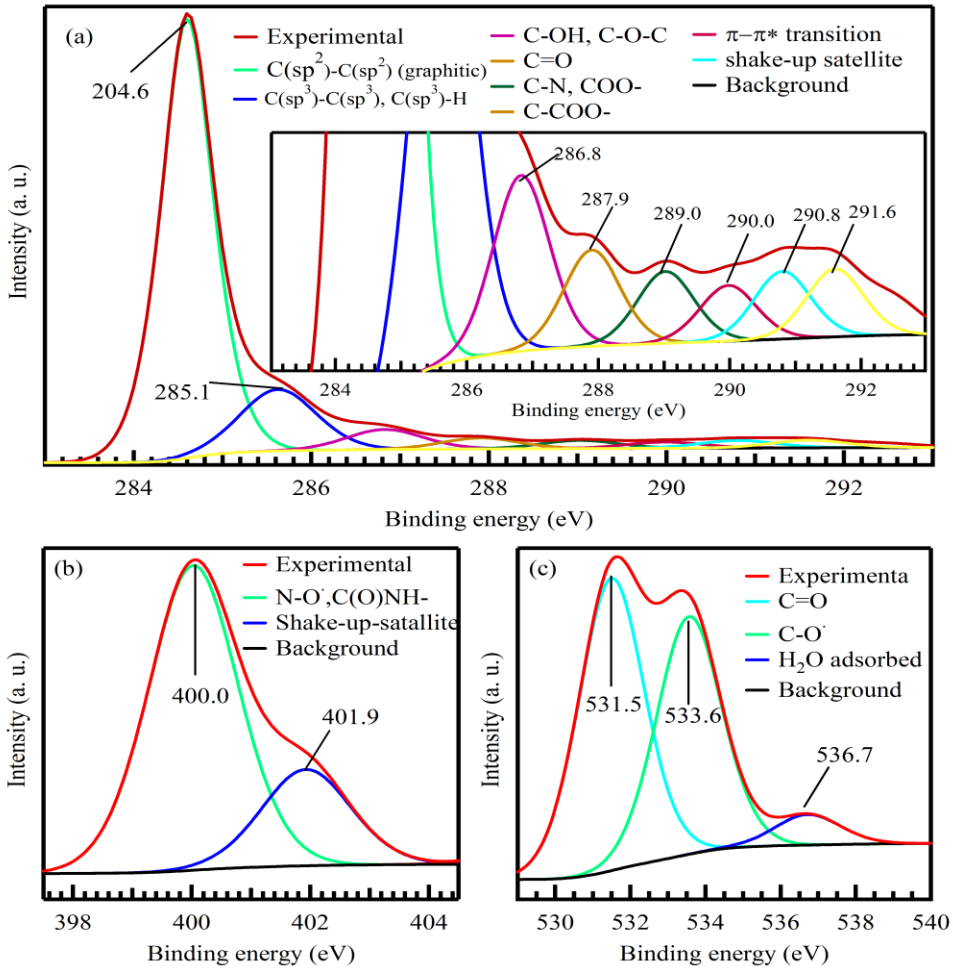

Fig. 1. XPS spectra of MWCNTs–TEMPO (**a**) C 1s, (**b**) N 1s and (**c**) O 1s.

FTIR spectra were recorded for MWCNTs and MWCNTs-TEMPO and they are shown in Fig. S6. As can be seen, the characteristic modes corresponding to the functional groups are clearly visible. In the spectrum of MWCNTs-TEMPO, the prominent bands which confirm the functional groups are as follows: 700-820 cm^{-1} (CH), 1047 cm^{-1} (OH), 1250 cm^{-1} (CN), 1380 cm^{-1} (>$NO^{\bullet}$), 1250 cm^{-1} (COOH), 1710 cm^{-1} (C=O), 2962 cm^{-1} (CH_3 from piperidine ring) and 3440-3850 cm^{-1} (NH in amide group) [55].

Fig. 2 depicts the results of TGA of MWCNTs and MWCNTs-TEMPO. The weight loss observed for MWCNTs-TEMPO in the range of temperature 150 - 500 ^{o}C corresponds to the

decomposition process of functional groups attached to the nanotube surfaces. It is clearly visible that the weight loss observed at this stage is greater in the case of MWCNTs-TEMPO than observed for MWCNTs. The thermal degradation at the temperatures higher than 600 ^{o}C corresponds to the thermal oxidation of disordered carbon [56]. The extra weight loss (14%) at 800 °C can be an indication for the amount of TEMPO groups that attached to the MWCNTs and this amount of TEMPO contributes significantly to the performance of MWCNTs-TEMPO as supercapacitor electrode.

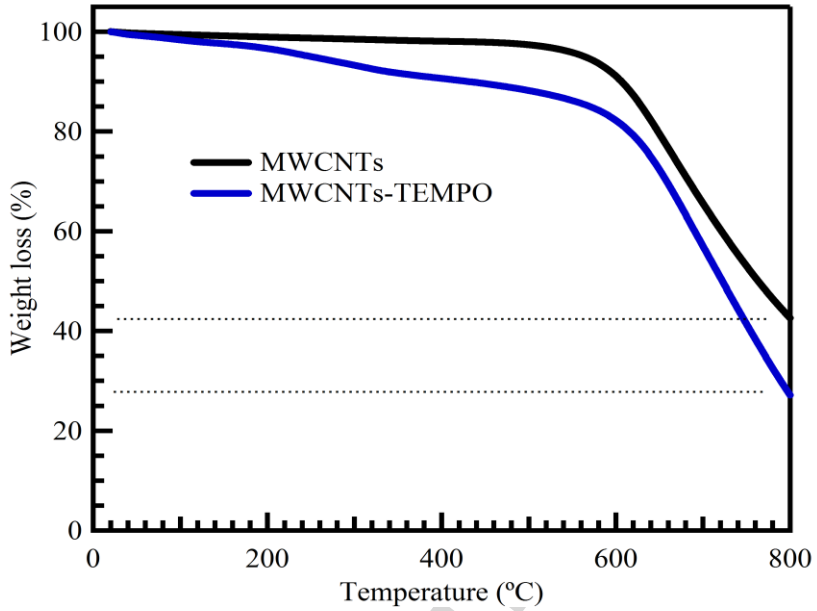

Fig. 2. TGA curves of MWCNTs and MWCNTs–TEMPO.

3.2. Electrochemical properties

3.2.1. Performance of the supercapacitor electrode

Fig. 3a shows the CV curves of MWCNTs and MWCNTs-TEMPO in 2 M KOH at 25 mV s^{-1}. It can be clearly seen that MWCNTs exhibits pure EDLC behavior by demonstrating large non-faradaic current between 0 and -1.0 V. For MWCNTs-TEMPO, similar EDLC behavior is also demonstrated, but with an additional pair of reversible redox peaks at -0.45/-

0.51 V that could be ascribed to the reversible nitroxide radical/aminoxyl anion (see Scheme 2) [57, 58].

Scheme 2. The reversible TEMPO redox reaction.

The diffusion behavior of these redox peaks are evaluated by scanning voltammetry at different scan rates (Fig. 3b). As the scan rate increases, both of the corresponding redox faradaic and non-faradaic currents increase, which indicate faster K^+ ions diffusion onto MWCNTs-TEMPO surface. The redox faradaic current is further investigated and it is found that the anodic peak current is directly proportional to the square root of scan rate (Fig. 3c). This implies that the observed redox reaction is dominated by the K^+ ions diffusion process onto MWCNTs-TEMPO surface. The diffusion coefficient (D) of K^+ ion is calculated using the slope of Fig. 3c based on Randles-Sevcik equation [25]:

$$i_P = 2.69 \times 10^5 \, n^{3/2} \, S_A \, D^{1/2} \, C \, v^{1/2} \quad (1)$$

where i_p is the peak current (A), n is the number of electrons in the redox reaction (according to Scheme 2, n = 1), S_A is the electrode area (cm^2), C is the concentration of the electroactive species at the electrode (g cm^{-3}) and v is the scan rate (V s^{-1}). D is computed to be 2.6×10^{-7} cm^2 s^{-1} which shows fast K^+ ions diffusion as a result of wider pores diameter of 15.1 nm (this value is comparable to the reported values for K^+ in different electrode materials [59, 60]). Fig. 3d shows the CDC curves of MWCNTs and MWCNTs-TEMPO. Similar as CV findings, the CDC of MWCNTs shows pure EDLC behavior by having linear CDC curves, while MWCNTs-TEMPO demonstrates additional pseudocapacitive behavior by having curve shoulder at ca. -0.4 V which corresponds to the redox reaction of nitroxide radical/aminoxyl anion. The CDC curves of MWCNTs-TEMPO at different current densities are shown in Fig. 3e. The charge and discharge times for MWCNTs-TEMPO are prolonged at lower CDC current densities, which is attributed to the slow voltage build up at low current densities that allows K^+ ions to have more time to diffuse towards to the MWCNTs-TEMPO surface. The specific capacitance of the samples are calculated by dividing the current densities with the CDC slope and summarized as Fig. 3f. Both MWCNTs and MWCNTs-TEMPO exhibit similar

trend to have higher specific capacitance at lower current densities. As explained in CDC analyses, at low current density, the K^+ ions have sufficient time to diffuse to the MWCNTs-TEMPO surface and consequently to have more K^+ ions on the MWCNTs-TEMPO surface. The highest specific capacitance for MWCNTs-TEMPO is calculated to be 66 F g^{-1} at 0.25 A g^{-1}, ca. 5 times higher as compared to that of MWCNTs (13.5 F g^{-1} at 0.25 A g^{-1}). Similar capacitance enhancement is also demonstrated by other works where TEMPO radical was incorporated into electrolyte for the anodic [39] or cathodic [57] redox reaction. However, to the best of our knowledge, the functionalization of electrode with TEMPO moiety is first being demonstrated in this work. Due to the MWCNTs used in this work is produced as industrial grade product, MWCNTs possesses low specific capacitance as the quality is often compromised during industrial production. However, the facile functionalization to produce pseudocapacitive MWCNTs-TEMPO can enhance the specific capacitance up to 5 times.

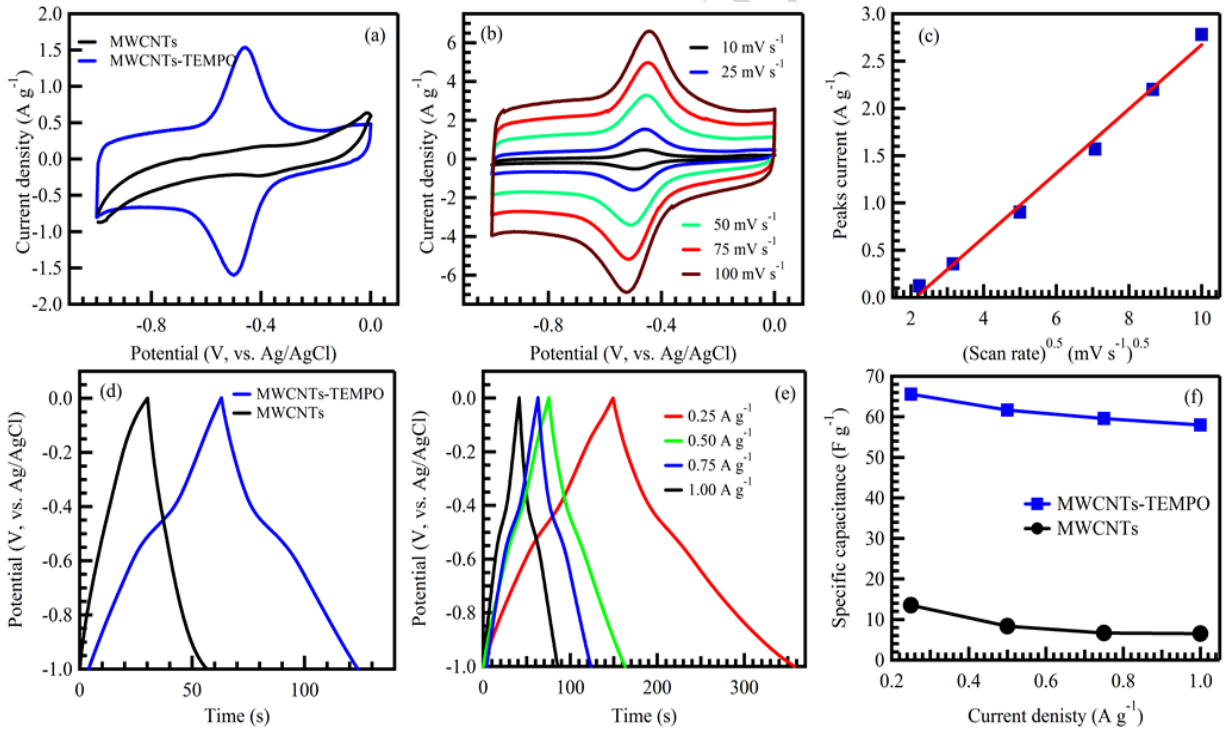

Fig. 3. Cyclic voltammetry at 25 mV s^{-1} of MWCNTs and MWCNTs–TEMPO (**a**), at different scan rates of MWCNTs–TEMPO (**b**), peaks current as a function of square rote of scan rate of MWCNTs–TEMPO (**c**), charge–discharge curves at 0.75 A g^{-1} of MWCNTs and MWCNTs–TEMPO (**d**), at different current densities of MWCNTs–TEMPO (**e**) and specific capacitance as a function current density (**f**) of MWCNTs and MWCNTs–TEMPO electrodes in 2 M KOH.

Fig. 4a shows Nyquist plot for MWCNTs-TEMPO at open circuit potential (OCP) in 2 M KOH, the inset shows the zoomed view of the high-frequency region of the Nyquist plot. The Nyquist plot shows a small semi-circle in the high-frequency region and a vertical line at low frequency, which represents the dominance of capacitive behavior from the formation of ionic and electronic charges of the electric double layer system at the MWCNTs-TEMPO electrode surface [61]. The phase angle MWCNTs-TEMPO is found to be 80° (see Bode plot in Fig. 4b), which is close to ideal supercapacitor (90°) [51]. The experimental data for MWCNTs (Fig. S7a-b) and MWCNTs-TEMPO are fitted by equivalent circuit fitting and the results are summarized as Table 1. The solution resistance (R_s), or better known as the equivalent series resistance (ESR) represent the intrinsic conductivity of the electrode material. As mentioned earlier, industrial-grade MWCNTs possesses low conductivity (R_s of 3.77 Ω), and significant improvement can be seen upon functionalization in MWCNTs-TEMPO which shows improved conductivity (R_s of 0.67 Ω). R_s was found to be lower than reported values for MWCNT-aromatic azides (3.60 Ω) [62], MWCNT/PANI (1.54 Ω), TiO_2-MWCNT/PANI (1.16 Ω) and graphene/TiO_2-MWCNT/PANI (1.12 Ω) [63]. In addition, MWCNTs-TEMPO also demonstrates enhanced charge transfer resistance (R_{ct} of 0.08 Ω) as compared to that of MWCNTs (R_{ct} of 0.44 Ω), indicating facile electron transfer across electrode-electrolyte interface during redox process. The R_{ct} is lower than other reported values for MWCNT/PANI (24.60 Ω) [63], graphene/TiO_2-MWCNT/PANI (23.64 Ω) [63], TiO_2-MWCNT/PANI (13.47 Ω) [63], unzipped MWCNTs (8.71 Ω) [64], MWCNTs (5.13 Ω) [51], MWCNTs-GO (1.12 Ω) [51], MWCNT-aromatic azides (0.70 Ω) [62] and MWCNTs-Cyst (0.18 Ω) [13]. Both enhancements can be associated to the unpaired electron from TEMPO.

The electrochemical active surface area (S_E) can be calculated from EIS findings as reported elsewhere [21, 65]. The calculated S_E value for MWCNTs-TEMPO is found to 180.4 $m^2\ g^{-1}$, which is higher than that of MWCNTs (45.9 $m^2\ g^{-1}$) and indicates the high electrochemical active surface area of MWCNTs-TEMPO electrode. These findings are in good agreement with those obtained from BET data as MWCNTs-TEMPO shows high S_{BET} of 55.7 $m^2\ g^{-1}$ and high pore diameter of 15.1 nm. The higher electrochemical active surface area in MWCNTs-TEMPO can be attributed to the presence of redox-active TEMPO group and the separated nanotubes morphology as seen in HRTEM. Consequently, higher electrochemical

active surface area is the determining factor in higher specific capacitance of MWCNTs-TEMPO.

The relaxation time ($\tau = {}^{1}/_{f_o}$) was calculated from the capacitor response frequency (f_o) corresponding to the phase angle of 45°. MWCNTs-TEMPO shows τ values of 0.47 s, indicating the good electrochemical capacitance properties, and fast charge-discharge characteristic response. The τ value distinguishes the transition between resistive and capacitive behaviors, as it defines predominantly resistive behavior at frequencies above $1/\tau$ and capacitive behavior below $1/\tau$. The τ of the present sample is lower than 8 s found for activated carbon-based electrodes and 4.9 s obtained for carbon nanotubes in other works [21, 66, 67].

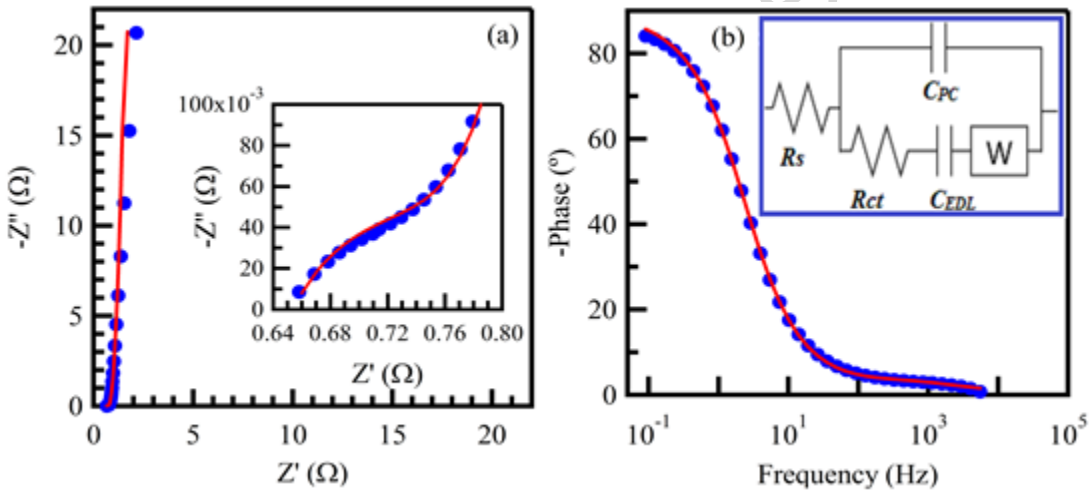

Fig. 4. Nyquist (**a**) and Bode (**b**) plots: the insets of (**a**) is the curves at the high–frequency region and (**b**) is the equivalent circuit fitting (the solid lines are the fitting results) for MWCNTs–TEMPO electrode in 2 M KOH.

Table 1. Fitting parameters of the experimental impedance data for MWCNTs and MWCNTs–TEMPO electrode in 2 M KOH.

	Rs ***(Ω)***	***R_{ct}*** ***(Ω)***	***C_{PC}*** ***(mF)***	***C_{EDL}*** ***(mF)***	***W*** ***(Ω)***	***S_E*** ***($cm^2\ g^{-1}$)***	***τ*** ***(s)***
MWCNTs–TEMPO	0.67	0.08	2.7	86.1	1.01	180.4	0.47

MWCNTs	3.77	0.44	0.1	4.6	0.05	45.9	0.12

3.2.2. Performance of the symmetrical supercapacitor

The energy stored in a supercapacitor is directly proportional to the capacitance and the operating voltage, therefore increasing the operating voltage of a supercapacitor is highly crucial. Generally, the working potential window is limited by the nature of the electrode material and the electrolytes [68, 69]. It is known that, in KOH solution, the electrode can work in the range from -1 to 0.5 V, so the complete cell in symmetric supercapacitor can work up to 1.5 V. On the other hand, in Na_2SO_4 solution, it can work in the range from -1 to 1 V, and accordingly, the complete cell can work up to 2 V. For this purpose the symmetric supercapacitor was tested in both electrolytes to investigate the potential window stability. Fig. 5a-b shows CV curves in 2 M KOH in the potential range of 0-1 V and 0-1.6 V, respectively, at different scan rates of MWCNTs-TEMPO symmetric supercapacitor. Meanwhile, the symmetric supercapacitor shows a wider operating potential range of 2 V in Na_2SO_4 as shown in Fig. 5c-f. It shows a rectangular CV shapes in all potential windows indicating that it could be applied to higher potentials and store more energy.

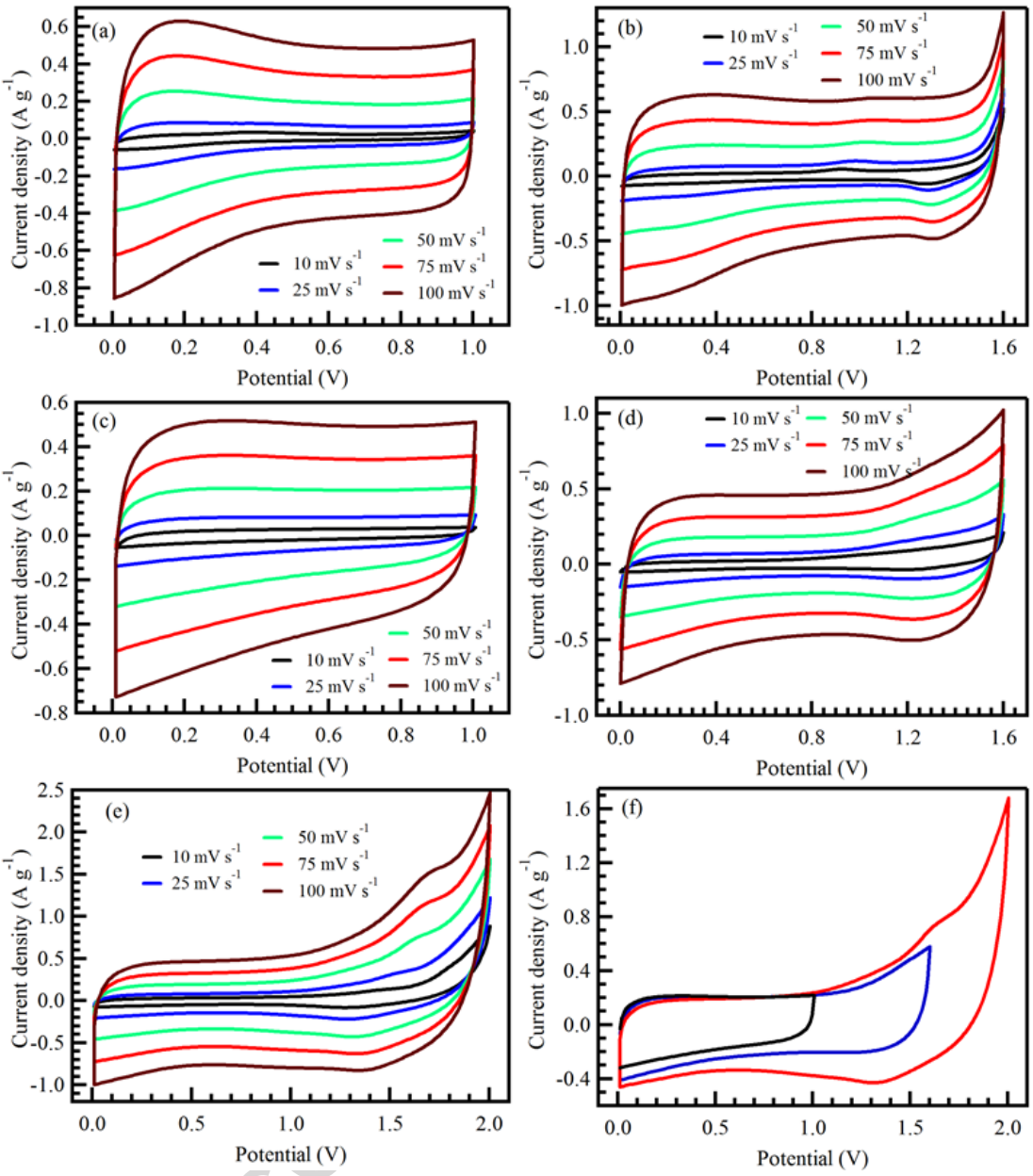

Fig. 5. Cyclic voltammetry curves at different scan rates under 0–1 V (**a**) and 0–1.6 V (**b**) in 2 M KOH, 0–1 V (**c**), 0–1.6 V (**d**), 0–2 V (**e**) and under different potential windows at 50 mV s^{-1} (**d**) in 1 M Na_2SO_4 for the symmetric supercapacitor.

The operating voltage window stability of the symmetric supercapacitor was further tested by galvanostatic CDC. Fig. 6a-c shows the CDC curves in 2 M KOH solution in the potential ranges up to 1.6 V for different current densities. Linear charge and discharge curves with neglected *iR* drop are obtained, which indicates the low internal resistance of electrodes which leads to better capacitive performance. Moreover, as shown in Fig. 6d, the specific

capacitance was found to be 55, 43 F g^{-1} at 0.25 A g^{-1} for 1.6 V and 1 V, respectively. The inset of Fig. 6d shows the increment of specific capacitance values with increasing voltage window. These findings are much higher than those obtained for non-functionalized MWCNTs in other work (10 F g^{-1}) [70].

On the other hand, the symmetric supercapacitor shows wider potential window up to 2 V in a neutral electrolyte (Na_2SO_4) as shown in Fig. 7a-e. The CDC curves are more linear in Na_2SO_4 than in KOH due to lower pseudocapacitance contribution in the neutral electrolyte [71]. The symmetric supercapacitor shows a specific capacitance of 48, 36 and 33 F g^{-1} at 0.25 A g^{-1} for 2, 1.6 and 1 V, respectively. These findings are higher than those obtained for cysteamine functionalized MWCNTs symmetric supercapacitor (23 F g^{-1} at 0.25 A g^{-1}) and MWCNTs symmetric supercapacitor (6 F g^{-1} at 0.25 A g^{-1}) [13]. In KOH, the symmetric supercapacitor shows higher specific capacitance values than in Na_2SO_4, that could be attributed to (1) the radius of hydration sphere of K^+ (3.31 Å) is lower than Na^+ (3.58 Å), (2) the molar conductivity of K^+ (73.5 cm^2 Ω^{-1} mol^{-1}) is higher than Na^+ (50.1 cm^2 Ω^{-1} mol^{-1}) and the mobility of K^+ (7.6×10^{-5} cm^2 S^{-1} V^{-1}) is higher than Na^+ (5.2×10^{-5} cm^2 S^{-1} V^{-1}) [45]. All these factors contribute to faster K^+ ions mobility within the structure and therefore storing more charges.

The energy and power densities can be calculated from CDC data using equations reported elsewhere [39]. Ragone plot (energy density vs. power density) of the symmetric supercapacitor is shown in Fig. 7f. Under the similar potential window at 1.6 V, the supercapacitor shows higher energy density of 21.4 Wh kg^{-1} at a power density of 893.4 W kg^{-1} in KOH, as compared to that in Na_2SO_4 (energy density of 12.8 Wh kg^{-1} at a power density of 886.2 W kg^{-1}). Nonetheless, by increasing potential window up to 2 V, which is unachievable in KOH, the supercapacitor with Na_2SO_4 shows high energy density of 26.6 Wh kg^{-1} at a power density of 1168.2 W kg^{-1}. These findings are much higher than those obtained for supercapacitors fabricated from non-functionalized MWCNTs (2.2 Wh kg^{-1}) [70], activated carbon (4 Wh kg^{-1}) [72] carbon nanospheres from biowaste sago bark (5 Wh kg^{-1}) [22], graphene nanosheet (5 Wh kg^{-1}) [21], porous nanocarbons from oil palm leaves (10-13 Wh kg^{-1}) [73, 74], MnO_2/graphene (16 Wh kg^{-1}) [75] (more comparison can be referred to Table S1).

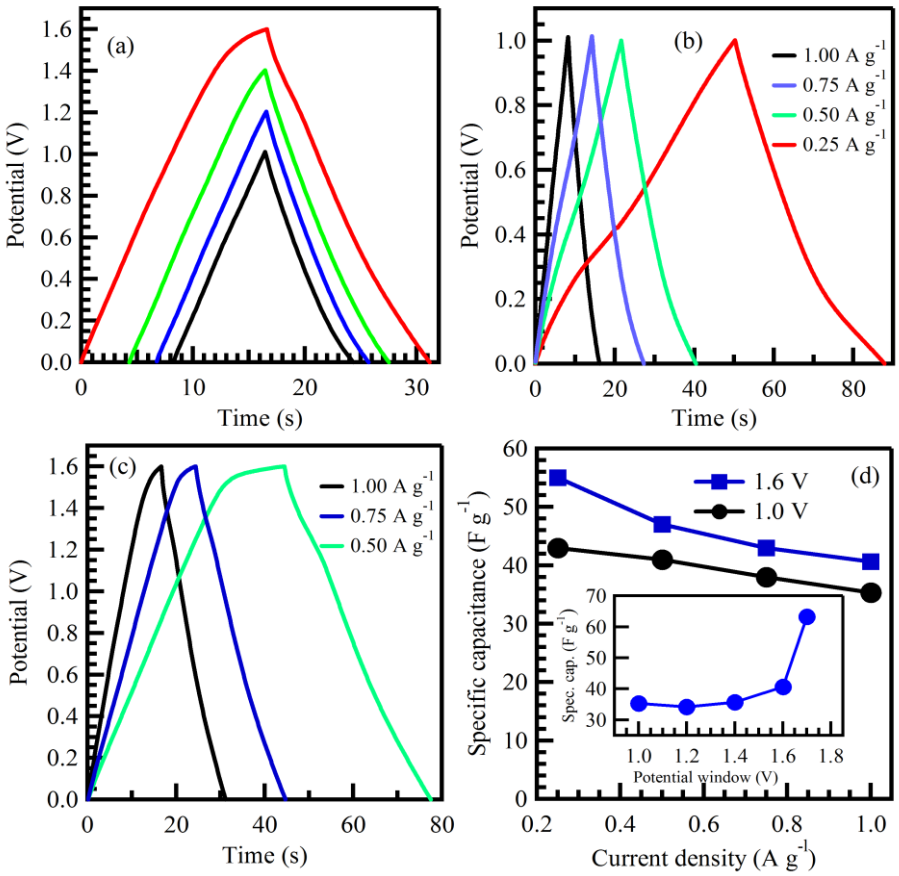

Fig. 6. Charge–discharge curves at 1 A g^{-1} under different potential windows (**a**), at different current densities under 1 V (**b**), 1.6 V (**c**) and specific capacitance as a function of current density (**d**) for symmetric supercapacitor in 2 M KOH: Inset of (**d**) specific capacitance as a function of potential window.

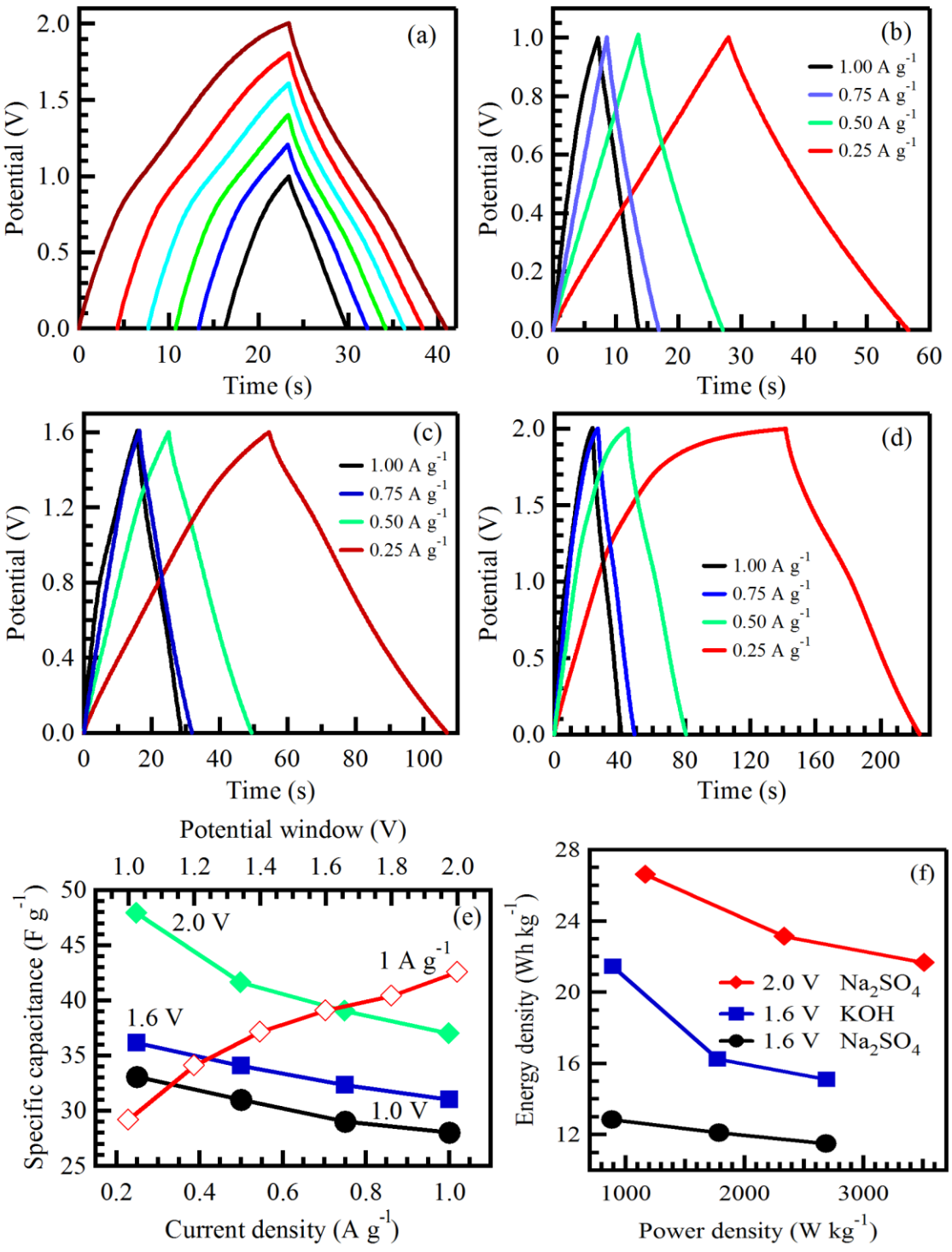

Fig. 7. Charge–discharge curves at 1 A g^{-1} under different potential windows (**a**), at different current densities under 1 V (**b**), 1.6 V (**c**), 2 V (**d**), specific capacitance as a function of potential window and current density (**e**) and Ragone plots (**f**) of the symmetric supercapacitor in 1 M Na_2SO_4.

The cycling stability is a momentous characteristic for a supercapacitor [69]. The cycling stability of the symmetric supercapacitor was tested at 0.5 A g^{-1} for up to 4000 CDC cycles in KOH and Na_2SO_4 as shown in Fig. 8a-b. MWCNTs-TEMPO shows high cyclic stability of 86% (in KOH) and 90% (in Na_2SO_4) for 4000 CDC cycles. In addition, the Coulombic efficiency was found to be 91% (in KOH) and 92% (in Na_2SO_4) at the end of CDC. The insets of Fig. 8 show the CDC curves at the representative cycles to indicate the insignificant change of the curves even after these long cycling process. The high cycling stability is a motivating factor for using this material in the supercapacitor application.

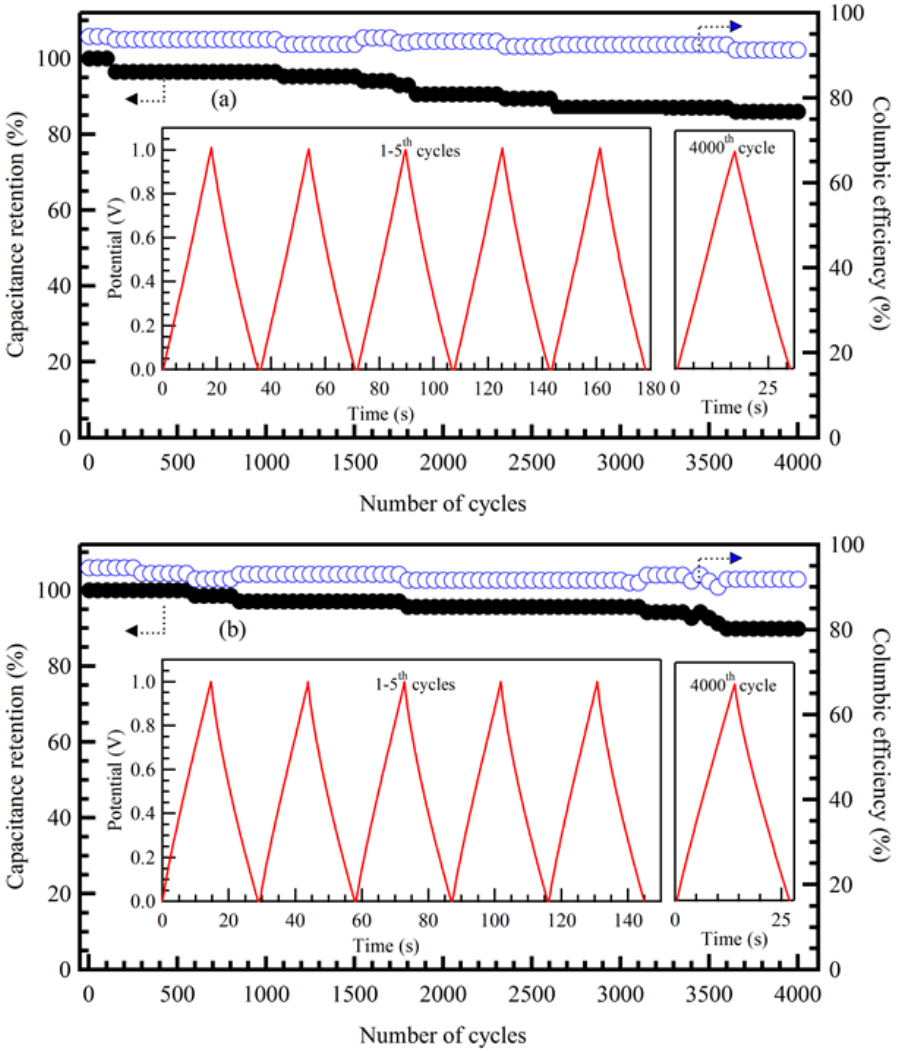

Fig. 8. Cycle life stability (left vs. bottom) and Coulombic efficiency (right vs. bottom) at 0.5 A g^{-1} for symmetric supercapacitor, the insets show the charge–discharge curves for different cycles in 2 M KOH (**a**) and 1 M Na_2SO_4 (**b**).

4. Conclusions

In summary we developed a new protocol for functionalizing MWCNTs with electrochemically active TEMPO moieties. The prepared material (MWCNTs-TEMPO) is tested electrochemically (CV, CDC and EIS) as a supercapacitor electrode and shows capacitive characteristics with pseudocapacitance contribution. The specific capacitance of the functionalized MWCNTs-TEMPO is found to be 5-times higher than the MWCNTs, indicating the improvement of the electrochemical characteristics of the industrial grade MWCNTs. The symmetric supercapacitor fabricated from MWCNTs-TEMPO shows a superior behavior in a wide potential range up to 2 V, high cyclic stability reaching up 90% retention and Coulombic efficiency of 92% over 4000 cycles as well as high energy density of 26.6 Wh kg^{-1}. Such characteristics clearly indicate that the MWCNTs-TEMPO can be successfully used as high efficient supercapacitor electrode.

Conflicts of interest

There are no conflicts to declare

Acknowledgments

This work was financially supported by the National Science Centre of Poland (NCN grant No. DEC-2013/09/B/ST5/00988). In addition, the authors would like to acknowledge the funding from the Ministry of Education Malaysia FRGS [RDU160118: FRGS/1/2016/STG07/UMP/02/3] and Universiti Malaysia Pahang [grant number RDU170357]. Moreover, the authors extend their appreciation to the Deanship of Scientific Research at King Khalid University for funding this work through research groups program under grant number (R.G.P.2/2/38). The authors thank Grzegorz Cichowicz (M.Sc.) University of Warsaw, Faculty of Chemistry for performing XRD measurements.

References

[1] S. Iijima, Helical microtubules of graphitic carbon, Nature, 354 (1991) 56–58.

[2] H. Sadegh, R. Shahryari–ghoshekandi, M. Kazemi, Study in synthesis and characterization of carbon nanotubes decorated by magnetic iron oxide nanoparticles, Int. Nano Lett., 4 (2014) 129–135.

[3] K. Zare, H. Sadegh, R. Shahryari–ghoshekandi, B. Maazinejad, V. Ali, I. Tyagi, S. Agarwal, V.K. Gupta, Enhanced removal of toxic Congo red dye using multi walled carbon nanotubes: Kinetic, equilibrium studies and its comparison with other adsorbents, J. Mol. Liq., 212 (2015) 266–271.

[4] Z. Liu, Z. Shen, T. Zhu, S. Hou, L. Ying, Z. Shi, Z. Gu, Organizing single–walled carbon nanotubes on gold using a wet chemical self–assembling technique, Langmuir, 16 (2000) 3569–3573.

[5] R.K. Abu Al–Rub, A.I. Ashour, B.M. Tyson, On the aspect ratio effect of multi–walled carbon nanotube reinforcements on the mechanical properties of cementitious nanocomposites, Constr. Build. Mater., 35 (2012) 647–655.

[6] M. Mahmoodi, M. Arjmand, U. Sundararaj, S. Park, The electrical conductivity and electromagnetic interference shielding of injection molded multi-walled carbon nanotube/polystyrene composites, Carbon, 50 (2012) 1455–1464.

[7] M. Melchionna, S. Marchesan, M. Prato, P. Fornasiero, Carbon nanotubes and catalysis: the many facets of a successful marriage, Catal. Sci. Technol., 5 (2015) 3859–3875.

[8] K. Zare, V.K. Gupta, O. Moradi, A.S.H. Makhlouf, M. Sillanpää, M.N. Nadagouda, H. Sadegh, R. Shahryari–ghoshekandi, A. Pal, Z.J. Wang, A comparative study on the basis of adsorption capacity between CNTs and activated carbon as adsorbents for removal of noxious synthetic dyes: a review, J. Nanostruct. Chem., 5 (2015) 227–236.

[9] H. Sadegh, R. Shahryari–ghoshekandi, Functionalization of carbon nanotubes and its application in nanomedicine: A review, Nanomed. J., 2 (2015) 231–248.

[10] L. Valentini, C. Cantalini, L. Lozzi, I. Armentano, J.M. Kenny, S. Santucci, Reversible oxidation effects on carbon nanotubes thin films for gas sensing applications, Mater. Sci. Eng., C, 23 (2003) 523–529.

[11] R.J. Chen, S. Bangsaruntip, K.A. Drouvalakis, N. Wong Shi Kam, M. Shim, Y. Li, W. Kim, P.J. Utz, H. Dai, Noncovalent functionalization of carbon nanotubes for highly specific electronic biosensors, Proc. Natl. Acad. Sci. U.S.A., 100 (2003) 4984–4989.

[12] H. Pan, J. Li, Y.P. Feng, Carbon nanotubes for supercapacitor, Nanoscale Res. Lett., 5 (2010) 654–668.

[13] G.A.M. Ali, E.Y. Lih Teo, E.A.A. Aboelazm, H. Sadegh, A.O.H. Memar, R. Shahryari-Ghoshekandi, K.F. Chong, Capacitive performance of cysteamine functionalized carbon nanotubes, Mater. Chem. Phys., 197 (2017) 100–104.

[14] L.J. Brennan, M.T. Byrne, M. Bari, Y.K. Gun'ko, Carbon nanomaterials for dye–sensitized solar cell applications: A bright future, Adv. Energy Mater., 1 (2011) 472–485.

[15] A. Thess, R. Lee, P. Nikolaev, H. Dai, P. Petit, J. Robert, C. Xu, Y.H. Lee, S.G. Kim, A.G. Rinzler, Crystalline ropes of metallic carbon nanotubes, Science, 273 (1996) 483–487.

[16] R.J. Cartwright, S. Esconjauregui, R.S. Weatherup, D. Hardeman, Y. Guo, E. Wright, D. Oakes, S. Hofmann, J. Robertson, The role of the sp^2:sp^3 substrate content in carbon supported nanotube growth, Carbon, 75 (2014) 327–334.

[17] Z. Sarkozi, K. Kertesz, A.A. Koos, Z. Osvath, L. Tapaszto, Z.E. Horvath, P. Nemes-Incze, I.Z. Jenei, Z. Vertesy, N.S. Daroczi, A. Darabont, O. Pana, L.P. Biro, Synthesis of carbon nanotubes from liquid hydrocarbons using a spray–pyrolysis method, J. Optoelectron. Adv. Mater., 10 (2008) 2307–2310.

[18] B.M. Sun, W.H. Cao, Y.H. Guo, Y. Wang, J.T. Luo, P. Jiang, Flame pyrolysis synthesis of self–oriented carbon nanotubes, AIP Adv., 3 (2013) 092102–092109.

[19] F. Avilés, J. Cauich-Rodríguez, L. Moo–Tah, A. May–Pat, R. Vargas–Coronado, Evaluation of mild acid oxidation treatments for MWCNT functionalization, Carbon, 47 (2009) 2970–2975.

[20] A. Aqel, K.M.M.A. El-Nour, R.A.A. Ammar, A. Al–Warthan, Carbon nanotubes, science and technology part (I) structure, synthesis and characterisation, Arabian J. Chem., 5 (2012) 1–23.

[21] G.A.M. Ali, S.A. Makhlouf, M.M. Yusoff, K.F. Chong, Structural and electrochemical characteristics of graphene nanosheets as supercapacitor electrodes, Rev. Adv. Mater. Sci., 41 (2015) 35–43.

[22] G. Hegde, S.A. Abdul Manaf, A. Kumar, G.A.M. Ali, K.F. Chong, Z. Ngaini, K.V. Sharma, Biowaste sago bark based catalyst free carbon nanospheres: Waste to wealth approach, ACS Sustainable Chem. Eng., 3 (2015) 2247–2253.

[23] G.A.M. Ali, D. Aravind, S. Supriya, K.F. Chong, A. Ethiraj, M. Reddy, H. Gharni, G. Hegde, Carbon nanospheres derived from Lablab Purpureus as a high performance supercapacitor electrode: Green approach, Dalton Trans., 46 (2017) 14034–14044.

[24] G.A.M. Ali, M.M. Yusoff, K.F. Chong, Graphene Electrochemical production and its energy storage properties, ARPN J. Engin. Appl. Sc., 11 (2016) 9712–9717.

[25] P.E. Marina, G.A.M. Ali, L.M. See, E.Y.L. Teo, E.-P. Ng, K.F. Chong, In situ growth of redox–active iron–centered nanoparticles on graphene sheets for specific capacitance enhancement, Arabian J. Chem., DOI 10.1016/j.arabjc.2016.02.006(2016) doi:10.1016/j.arabjc.2016.1002.1006.

[26] N. Islam, J. Warzywoda, Z. Fan, Edge-oriented graphene on carbon nanofiber for high-frequency supercapacitors, Nano-Micro Lett., 10 (2017) 1–8.

[27] V.K. Gupta, A. Fakhri, S. Agarwal, M. Naji, Palladium oxide nanoparticles supported on reduced graphene oxide and gold doped: Preparation, characterization and electrochemical study of supercapacitor electrode, J. Mol. Liq., 249 (2018) 61–65.

[28] G. Lota, K. Fic, E. Frackowiak, Carbon nanotubes and their composites in electrochemical applications, Energy Environ. Sci., 4 (2011) 1592–1605.

[29] J. Zhang, L.-B. Kong, B. Wang, Y.-C. Luo, L. Kang, In-situ electrochemical polymerization of multi–walled carbon nanotube/polyaniline composite films for electrochemical supercapacitors, Synth. Met., 159 (2009) 260–266.

[30] J. Hu, L. Shi, J. Men, L. Wang, Synthesis of amorphous MnO_2/MWCNT nanocomposites and their electrochemical properties, Asian J. Chem., 26 (2014) 6279−6284.

[31] A.S. Adekunle, K.I. Ozoemena, B.B. Mamba, B.O. Agboola, O.S. Oluwatobi, Supercapacitive properties of symmetry and the asymmetry two electrode coin type supercapacitor cells made from MWCNTs/nickel oxide nanocomposite, Int. J. Electrochem. Sci., 6 (2011) 4760–4774.

[32] P. Bilalis, D. Katsigiannopoulos, A. Avgeropoulos, G. Sakellariou, Non–covalent functionalization of carbon nanotubes with polymers, RSC Adv., 4 (2014) 2911–2934.

[33] S. Kaur, N. Raravikar, B.A. Helms, R. Prasher, D.F. Ogletree, Enhanced thermal transport at covalently functionalized carbon nanotube array interfaces, Nat. Commun., 5 (2014) 3082–3090.

[34] Q.F. Pengfei, O. Vermesh, M. Grecu, A. Javey, O. Wang, H.J. Dai, S. Peng, K.J. Cho, Toward large arrays of multiplex functionalized carbon nanotube sensors for highly sensitive and selective molecular detection, Nano Lett., 3 (2003) 347–351.

[35] H. Sadegh, R. Shahryari–ghoshekandi, S. Agarwal, I. Tyagi, M. Asif, V.K. Gupta, Microwave–assisted removal of malachite green by carboxylate functionalized multi–walled carbon nanotubes: Kinetics and equilibrium study, J. Mol. Liq., 206 (2015) 151–158.

[36] R. Garcia–Gonzalez, A. Fernandez–La Villa, A. Costa–Garcia, M.T. Fernandez–Abedul, Dispersion studies of carboxyl, amine and thiol–functionalized carbon nanotubes for improving the electrochemical behavior of screen printed electrodes, Sens. Actuators, B, 181 (2013) 353–360.

[37] S.K. Park, Q. Mahmood, H.S. Park, Surface functional groups of carbon nanotubes to manipulate capacitive behaviors, Nanoscale, 5 (2013) 12304–12309.

[38] L. Zhang, V.U. Kiny, H. Peng, J. Zhu, R.F.M. Lobo, J.L. Margrave, V.N. Khabashesku, Sidewall functionalization of single–walled carbon nanotubes with hydroxyl group–terminated moieties, Chem. Mater., 16 (2004) 2055–2061.

[39] E. Mourad, L. Coustan, P. Lannelongue, D. Zigah, A. Mehdi, A. Vioux, Stefan A. Freunberger, F. Favier, O. Fontaine, Biredox ionic liquids with solid-like redox density in the liquid state for high-energy supercapacitors, Nat. Mater., 16 (2016) 446–453.

[40] L. Tebben, A. Studer, Nitroxides: applications in synthesis and in polymer chemistry, Angew. Chem. Int. Ed., 50 (2011) 5034–5068.

[41] E. Megiel, Surface modification using TEMPO and its derivatives, Adv. Colloid Interface Sci., 250 (2017) 158–184.

[42] X.-D. Zhao, X.-H. Fan, X.-F. Chen, C.-P. Chai, Q.-F. Zhou, Surface modification of multiwalled carbon nanotubes via nitroxide-mediated radical polymerization, J. Polym. Sci., Part A: Polym. Chem., 44 (2006) 4656–4667.

[43] C. Yang, M. Guenzi, F. Cicogna, C. Gambarotti, G. Filippone, C. Pinzino, E. Passaglia, N.T. Dintcheva, S. Carroccio, S. Coiai, Grafting of polymer chains on the surface of carbon nanotubes via nitroxide radical coupling reaction, Polym. Int., 65 (2016) 48–56.

[44] P. Ionita, A. Caragheorgheopol, B.C. Gilbert, V. Chechik, Dipole−dipole interactions in spin-labeled Au nanoparticles as a measure of interspin distances, J. Phys. Chem. B, 109 (2005) 3734–3742.

[45] F. Barzegar, D. Momodu, O. Fashedemi, A. Bello, J. Dangbegnon, N. Manyala, Investigation of different aqueous electrolytes on the electrochemical performance of activated carbon-based supercapacitors, RSC Adv., 5 (2015) 107482–107487.

[46] S. Sankal, C. Kaynak, Using various techniques to characterize oxidative functionalized and aminosilanized carbon nanotubes for polyamide matrix, J. Reinf. Plast. Compos., 32 (2013) 75–86.

[47] O.A. Fouad, S.A. Makhlouf, G.A.M. Ali, A.Y. El-Sayed, Cobalt/silica nanocomposite via thermal calcination-reduction of gel precursors, Mater. Chem. Phys., 128 (2011) 70–76.

[48] O.A. Fouad, G.A.M. Ali, M.A.I. El-Erian, S.A. Makhlouf, Humidity sensing properties of cobalt oxide/silica nanocomposites prepared via sol-gel and related routes, Nano, 7 (2012) 1250038–1250049.

[49] Y.I. Avila-Vega, C.C. Leyva-Porras, M. Mireles, M. Quevedo-López, J. Macossay, J. Bonilla-Cruz, Nitroxide–functionalized graphene oxide from graphite oxide, Carbon, 63 (2013) 376–389.

[50] H. Ago, T. Kugler, F. Cacialli, W.R. Salaneck, M.S. Shaffer, A.H. Windle, R.H. Friend, Work functions and surface functional groups of multiwall carbon nanotubes, J. Phys. Chem. B, 103 (1999) 8116–8121.

[51] S.H. Aboutalebi, M. Salari, K. Konstantinov, D. Wexler, H.K. Liu, S.X. Dou, Comparison of GO, GO–MWCNTs composite, Energy Environ. Sci., 4 (2011) 1855–1865.

[52] O. Swiech, R. Bilewicz, E. Megiel, TEMPO coated Au nanoparticles: synthesis and tethering to gold surfaces, RSC Adv., 3 (2013) 5979–5986.

[53] K. Zawada, W. Tomaszewski, E. Megiel, A smart synthesis of gold/polystyrene core–shell nanohybrids using TEMPO coated nanoparticles, RSC Adv., 4 (2014) 23876–23885.

[54] M. Gozdziewska, G. Cichowicz, K. Markowska, K. Zawada, E. Megiel, Nitroxide-coated silver nanoparticles: synthesis, surface physicochemistry and antibacterial activity, RSC Adv., 5 (2015) 58403–58415.

[55] M. Wang, C. Shao, S. Zhou, J. Yang, F. Xu, Preparation of carbon aerogels from TEMPO-oxidized cellulose nanofibers for organic solvents absorption, RSC Adv., 7 (2017) 38220–38230.

[56] P. Hou, C. Liu, Y. Tong, S. Xu, M. Liu, H. Cheng, Purification of single-walled carbon nanotubes synthesized by the hydrogen arc-discharge method, J. Mater. Res., 16 (2001) 2526–2529.

[57] W. Guo, S. Xin, M. Ji, Y. Guo, L. Wan, Supercapacitor-battery hybrid energy storage devices from an aqueous nitroxide radical active material, Chin. Sci. Bull., 56 (2011) 2433–2436.

[58] J.B. Gerken, Y.Q. Pang, M.B. Lauber, S.S. Stahl, Structural effects on the pH-dependent redox properties of organic nitroxyls: Pourbaix diagrams for TEMPO, ABNO, and three TEMPO analogs, J. Org. Chem., 83 (2017) 7323–7330.

[59] Y. Zhou, F. Hou, Z.-P. Wan, Y.-L. Tang, D.-M. Yang, S. Zhao, R. Peng, Facile synthesis of $Ni(OH)_2$ nanoflakes on carbon nanotube films as flexible binder-free electrode for supercapacitors, ECS Solid State Lett., 3 (2014) 1–4.

[60] H. Kahlert, U. Retter, H. Lohse, K. Siegler, F. Scholz, On the determination of the diffusion coefficients of electrons and of potassium ions in copper (II) hexacyanoferrate (II) composite electrodes, J. Phys. Chem. B, 102 (1998) 8757–8765.

[61] F. Barzegar, A. Bello, J.K. Dangbegnon, N. Manyala, X. Xia, Asymmetric supercapacitor based on activated expanded graphite and pinecone tree activated carbon with excellent stability, Appl. Energy, 207 (2017) 417–426.

[62] S.K. Ujjain, R. Bhatia, P. Ahuja, P. Attri, Highly conductive aromatic functionalized multi-walled carbon nanotube for inkjet printable high performance supercapacitor electrodes, PLoS One, 10 (2015) 1–12.

[63] D. Ghosh, S. Giri, S. Kalra, C.K. Das, Synthesis and characterisations of TiO_2 coated multiwalled carbon nanotubes/graphene/polyaniline nanocomposite for supercapacitor applications, Open J. Appl. Sci., 2 (2012) 70–77.

[64] P. Sivaraman, S.P. Mishra, D.D. Potphode, A.P. Thakur, K. Shashidhara, A.B. Samui, A.R. Bhattacharyya, A supercapacitor based on longitudinal unzipping of multi-walled carbon nanotubes for high temperature application, RSC Adv., 5 (2015) 83546–83557.

[65] G.A.M. Ali, M.M. Yusoff, H. Algarni, K.F. Chong, One-step electrosynthesis of MnO_2/rGO nanocomposite and its enhanced electrochemical performance, Ceram. Int., 44 (2018) 7799–7807.

[66] C. Portet, P.L. Taberna, P. Simon, E. Flahaut, C. Laberty-Robert, High power density electrodes for carbon supercapacitor applications, Electrochim. Acta, 50 (2005) 4174–4181.

[67] Z. Bo, Z. Wen, H. Kim, G. Lu, K. Yu, J. Chen, One-step fabrication and capacitive behavior of electrochemical double layer capacitor electrodes using vertically-oriented graphene directly grown on metal, Carbon, 50 (2012) 4379–4387.

[68] F. Hekmat, B. Sohrabi, M. Rahmanifar, M. Vaezi, Supercapacitive properties of coiled carbon nanotubes directly grown on nickel nanowires, J. Mater. Chem., A, 2 (2014) 17446–17453.

[69] A. Balducci, D. Belanger, T. Brousse, J. Long, W. Sugimoto, Perspective-a guideline for reporting performance metrics with electrochemical capacitors: from eectrode materials to full devices, J. Electrochem. Soc., 164 (2017) 1487–1488.

[70] Y. Honda, T. Haramoto, M. Takeshige, H. Shiozaki, T. Kitamura, M. Ishikawa, Aligned MWCNT sheet electrodes prepared by transfer methodology providing high-power capacitor performance, Electrochem. Solid-State Lett., 10 (2007) 106–110.

[71] I. Aldama, V. Barranco, M. Kunowsky, J. Ibañez, J.M. Rojo, Contribution of cations and anions of aqueous electrolytes to the charge stored at the electric electrolyte/electrode interface of carbon-based supercapacitors, J. Phys. Chem. C, 121 (2017) 12053–12062.

[72] X.-J. Ma, W.-B. Zhang, L.-B. Kong, Y.-C. Luo, L. Kang, VO_2: from negative electrode material to symmetric electrochemical capacitor, RSC Adv., 5 (2015) 97239–97247.

[73] G.A.M. Ali, S.A.A. Manaf, D. A, K.F. Chong, G. Hegde, Superior supercapacitive performance in porous nanocarbons, J. Energy Chem., 25 (2016) 734–739.

[74] G.A.M. Ali, S.A. Abdul Manaf, A. Kumar, K.F. Chong, G. Hegde, High performance supercapacitor using catalysis free porous carbon nanoparticles, J. Phys. D: Appl. Phys., 47 (2014) 495307–495313.

[75] S. Deng, D. Sun, C. Wu, H. Wang, J. Liu, Y. Sun, H. Yan, Synthesis and electrochemical properties of MnO_2 nanorods/graphene composites for supercapacitor applications, Electrochim. Acta, 111 (2013) 707–712.

Graphical Abstract:

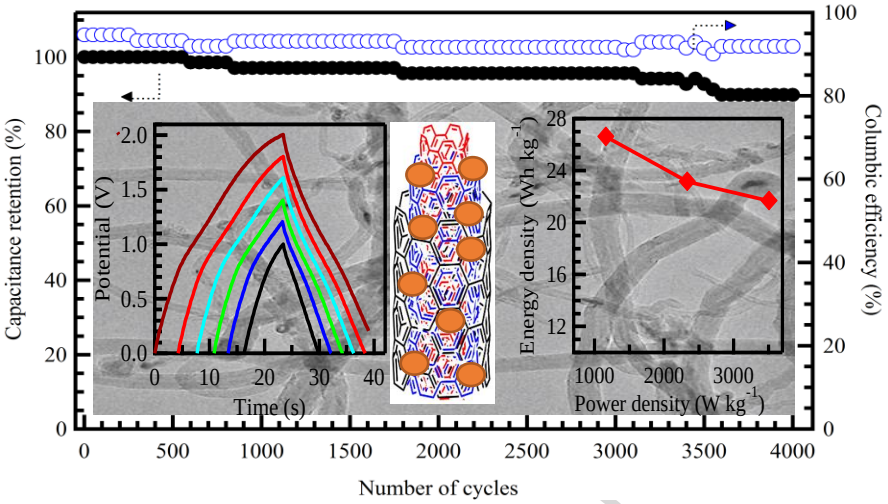

Highlights:

- MWCNTs is functionalized with TEMPO using a simple and effective method
- The effective coupling is confirmed by EPR, HRTEM, BET, XPS, FTIR and TGA
- The capacitive of MWCNTs–TEMPO is 5–times higher than the industrial grade MWCNTs
- The supercapacitor produces 26.6 Wh kg^{-1} with wide operating voltage 2 V
- The findings propose a facile approach to modify industrial grade MWCNTs